AGU PUBLICATIONS

JGR

Journal of Geophysical Research: Space Physics

RESEARCH ARTICLE

10.1002/2017JA023876

Key Points:
- A new electron density profile extrapolation technique (VCET), founded on First Principles, is presented showing a high performance
- VCET is simple and accurate: it is based on the linear behavior of the topside scale height, performing 6-20 times better than Chapman model
- The accuracy and extrapolation range, illustrated with FORMOSAT-3/COSMIC measurements, will be important for new radio-occultation missions like EPS-SG

Correspondence to:
M. Hernández-Pajares,
manuel.hernandez@upc.edu

Citation:
Hernández-Pajares, M., M. Garcia-Fernàndez, A. Rius, R. Notarpietro, A. von Engeln, G. Olivares-Pulido, À. Aragón-Àngel, and A. García-Rigo (2017), Electron density extrapolation above F2 peak by the linear Vary-Chap model supporting new Global Navigation Satellite Systems-LEO occultation missions, *J. Geophys. Res. Space Physics*, *122*, doi:10.1002/2017JA023876.

Received 7 JAN 2017
Accepted 11 JUL 2017
Accepted article online 20 JUL 2017

Electron density extrapolation above F2 peak by the linear Vary-Chap model supporting new Global Navigation Satellite Systems-LEO occultation missions

Manuel Hernández-Pajares[1], Miquel Garcia-Fernàndez[1,2], Antonio Rius[3], Riccardo Notarpietro[4], Axel von Engeln[4], Germán Olivares-Pulido[1,5], Àngela Aragón-Àngel[6], and Alberto García-Rigo[1]

[1]UPC-IonSAT, Barcelona, Spain, [2]Rokubun, Barcelona, Spain, [3]Instituto de Ciencias del Espacio (CSIC/IEEC), Bellaterra, Spain, [4]EUMETSAT, Darmstadt, Germany, [5]CRC for Spatial Information, Sydney, Australia, [6]European Commission, Joint Research Centre (JRC), Directorate for Space, Security and Migration, Ispra, Italy

Abstract The new radio-occultation (RO) instrument on board the future EUMETSAT Polar System-Second Generation (EPS-SG) satellites, flying at a height of 820 km, is primarily focusing on neutral atmospheric profiling. It will also provide an opportunity for RO ionospheric sounding, but only below impact heights of 500 km, in order to guarantee a full data gathering of the neutral part. This will leave a gap of 320 km, which impedes the application of the direct inversion techniques to retrieve the electron density profile. To overcome this challenge, we have looked for new ways (accurate and simple) of extrapolating the electron density (also applicable to other low-Earth orbiting, LEO, missions like CHAMP): a new Vary-Chap Extrapolation Technique (VCET). VCET is based on the scale height behavior, linearly dependent on the altitude above h_mF_2. This allows extrapolating the electron density profile for impact heights above its peak height (this is the case for EPS-SG), up to the satellite orbital height. VCET has been assessed with more than 3700 complete electron density profiles obtained in four representative scenarios of the Constellation Observing System for Meteorology, Ionosphere, and Climate (COSMIC) in the United States and the Formosa Satellite Mission 3 (FORMOSAT-3) in Taiwan, in solar maximum and minimum conditions, and geomagnetically disturbed conditions, by applying an updated Improved Abel Transform Inversion technique to dual-frequency GPS measurements. It is shown that VCET performs much better than other classical Chapman models, with 60% of occultations showing relative extrapolation errors below 20%, in contrast with conventional Chapman model extrapolation approaches with 10% or less of the profiles with relative error below 20%.

1. Introduction

The modeling and extrapolation of the electron density profiles in the ionosphere (hereinafter EDP) have recently received increased attention, in the context of new opportunities provided by satellite missions carrying on board a Global Navigation Satellite Systems (GNSS) radio-occultation receiver for the neutral atmospheric profiling, motivated by either ionospheric monitoring and space weather applications or by a better modeling of the ionospheric contribution to the bending angle [*Mannucci et al.*, 2011; *Danzer et al.*, 2015]. This is the case of the new European Organisation for the Exploitation of Meteorological Satellites (EUMETSAT) Polar System Second Generation (EPS-SG) satellites, covering the 2020 to 2040 time frame.

The main overall goal of the EPS-SG (consisting of three pairs of two satellites with 10 instruments each) is to provide global observations in order to derive information on variables of the atmosphere, ocean, and land, using sensors from low-Earth orbit (LEO) satellites. This will be done from polar orbits, providing global coverage and an expected significant positive impact on numerical weather prediction (NWP (see EPS-SG Web site, 2016, http://www.eumetsat.int/website/home/Satellites/FutureSatellites/EUMETSATPolarSystemSecondGeneration/EPSSGDesign/index.html)). The GNSS RO mission of the EPS-SG program (hereinafter RO-SG) will provide measurements of bending angle, almost vertical profiles of the troposphere and stratosphere, with high vertical resolution and accuracy, supporting NWP in near real time.

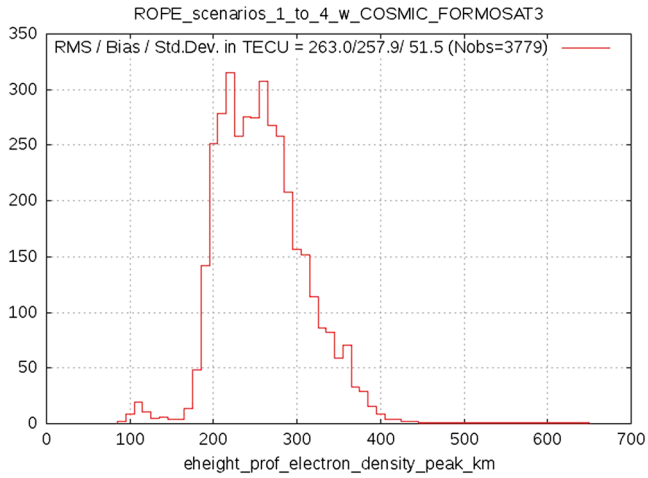

Figure 1. Distribution of EDP peak height values, h_mF_2, obtained by applying the updated IATI technique in the four scenarios considered in this work.

Additionally, the RO-SG will support space weather monitoring by providing information on key parameters of the Earth ionosphere: electron density (typically in terms of vertical profiles) and estimates of the associated vertical total electron content (VTEC). This will make use of the heritage of previous LEO-based RO missions of the Earth ionosphere and associated advances in modeling, since the pioneer GPS/MET [*Hajj and Romans*, 1998; *Rius et al.*, 1998; *Hernández-Pajares et al.*, 1998; *Ruffini et al.*, 1998; *Schreiner et al.*, 1999; *Hernández-Pajares et al.*, 2000], CHAMP [*Jakowski et al.*, 2002; *Garcia-Fernàndez et al.*, 2005a], the Satellite de Aplicaciones Cientificas-C (SAC-C) [*Garcia-Fernàndez associated et al.*, 2005b] and FORMOSAT-3/COSMIC [*Aragón-Àngel et al.*, 2011], among others, which all provide the RO measurements with straight line tangent altitude (SLTA — also known as straight line impact parameter, SLIP) below the corresponding LEO altitudes (approximately 740 km, 430 km, 715 km, and 800 km, respectively).

RO-SG, with its focus on the neutral atmosphere, will also provide radio-occultation measurements, intended for ionospheric profiling, from an orbital altitude of 820 km, but only for SLTA below 500 km approximately. This poses an extrapolation problem compared with the most of the previously mentioned missions which provided RO measurements with SLTA starting at the LEO height. Indeed, this creates a gap of RO measurements over more than 300 km, from 500 km up, which complicates the full estimation of the EDP up to the orbit height. The study of this problem, in particular the challenging electron density extrapolation up to the LEO height, is the main focus of this paper. Nevertheless, the RO-SG measurements available at such maximum SLTA value of 500 km will be, in almost all the cases, above the height of the electron density profile peak. The maximum corresponds typically to the F2 layer peak except for a few values around 100 km likely due to sporadic *E* layers, see Figure 1. And this is one of the improvements when comparing to the previous EPS RO GRAS receiver, which was providing only measurements for SLTA values below 80 km. This very low height range is adequate for neutral refractivity profiling, but it is missing almost all the direct measurements on the ionospheric profile below the satellite, see *Luntama* [2005]. In this context we focus on solving, in a simple and accurate way, the problem of the EDP extrapolation when direct RO measurements with SLTA above the EDP peak altitude are available. We will focus in this investigation on the future RO-SG by using data from FORMOSAT-3/COSMIC, with a similar satellite altitude (800 km).

The manuscript is structured in different sections, after this introduction: extrapolation of EDPs, VCET technique summary, data sets, results, and conclusions.

2. Extrapolation of Electron Density Profiles

The EDP modeling under the lack of RO data is typically performed by means of the standard Chapman model, defined by the peak height, h_mF_2, the peak electron density N_mF_2, and the scale height H, which is assumed constant in different works and modeling scenarios, such as (1) the topside of the profile: from in situ low-earth orbiting electron density measurements [see *Tulasi Ram et al.*, 2009], from radio-occultation measurements [see *Liu et al.*, 2008] or for combining GPS and ionosonde data in geomagnetic storm scenarios [*Zhu et al.*, 2016]; (2) the ionospheric and plasmaspheric modeling [see *González-Casado et al.*, 2015; *Lee et al.*, 2016; *Kutiev et al.*, 2016]; (3) the Multilayer Chapman model [*Alizadeh et al.*, 2015]; (4) the Ionospheric correction in tropospheric radio-occultation modeling [see *Danzer et al.*, 2015; *Zeng et al.*, 2016].

Recently, it has been shown [*Olivares-Pulido et al.*, 2016] that the topside ionosphere scale height (above h_mF_2 and up to ~700 km) is clearly not constant. This dependence on height is probably due to an imbalance

between the extreme ultraviolet (EUV) flux and the cooling scale time of electrons [*Su et al.*, 2015; *Olivares-Pulido et al.*, 2016]. Such imbalance would yield a systematic increase of the scale height with altitude, which could be approximated by a linear behavior, consistent with first principles (corresponding increase of the electron temperature in such ionospheric region), and also well described by the so-called Vary-Chap model [*Nsumei et al.*, 2012]. This has been demonstrated from EDPs globally distributed and derived from FORMOSAT-3/COSMIC GNSS RO phase observations [*Anthes et al.*, 2008] by means of the Improved Abel Transform Inversion (hereinafter IATI [see *Hernández-Pajares et al.*, 2000; *Garcia-Fernàndez et al.*, 2003; *Aragón-Àngel et al.*, 2011]). IATI is indeed more accurate than the standard Abel Transform Inversion, thanks to the incorporation in the ionospheric RO footprint of a horizontal gradient proxy (given by the variation of the vertical total electron content, VTEC, determined from global ground-based GPS observations).

In this context the main goal of this work is to show that the linear Vary-Chap model behaves like an accurate EDP topside extrapolation model (hereinafter Vary-Chap Extrapolation Technique, VCET) in the height range from 500 km up to the LEO height, which will be useful in particular for providing complete EDPs in future new opportunities of ionospheric sounding, such as the one provided by the RO instrument on board the EPS-SG mission. This will be demonstrated from raw dual-frequency GPS measurements gathered by the FORMOSAT-3/COSMIC LEO constellation, in four representative periods, including solar maximum, solar minimum, and extreme geomagnetic conditions.

3. The Vary-Chap Extrapolation Technique

The Vary-Chap Extrapolation Technique requires the electron density values directly derived at the topside of the EDP, from a height h_0 above the F2 maximum peak height (h_mF_2) up to the maximum height with available electron density estimation, h_1. Then, the VTEC extrapolation from h_1 up to the LEO GNSS receiver height h_2, can be performed following these steps:

1. It is assumed that the EDP has been estimated up to the maximum available height, h_1, with a reasonable accuracy (this might be achieved by applying direct data assimilation, such as *Hernández-Pajares et al.* [1998] or adapting the IATI introduced above).
2. The EDP peak value and height, N_mF_2 and h_mF_2, corresponding typically to the predominant F2 layer are identified.
3. A local α-Chapman model, without any assumption about the scale height H but with EDP peak value and height fixed to observed h_mF_2 and N_mF_2, is considered (equation (1)). In this way we can iteratively estimate the *local* scale height, H:

$$N_e(h) = N_mF_2 \cdot e^{\frac{1}{2}\left(1-z-e^{-z}\right)} \tag{1}$$

where $z = \frac{h-h_mF_2}{H}$, leading to the recursive equation to determine the local-scale height H at height h:

$$z_{k+1} = 1 - 2 \cdot \ln\left(\frac{N_e(h)}{N_mF_2}\right) - e^{-z_k} \tag{2}$$

4. The estimated scale height values H for each SLTA height, h, is given by $H = \frac{h-h_mF_2}{z^\star}$, where $z^\star$ is the final solution of equation (2), and the typical linear dependence of H, empirically found and justified in *Olivares-Pulido et al.* [2016], allows an accurate linear fit on h, in the available topside range within $[h_0, h_1]$.
5. The linearly extrapolated values of the scale height to the range $[h_1, h_2]$ are used, by means of the α-Chapman (equation (1)), to compute the electron density.
6. Finally, the extrapolated electron density values are assessed, taking as reference the electron density values directly retrieved from dual-frequency GPS RO measurements provided by the constellation of 6 FORMOSAT-3/COSMIC LEO satellites, in four representative data sets. This is done, in particular, by computing the error RMS for the extrapolated part of the EDP for every radio-occultation event.

4. Representative Data Sets

In order to capture as much as possible the different aspects of the ionospheric morphology, four different scenarios, listed in Table 1, have been set for this study. As far as the ionosphere is concerned, the relevant indices for each scenario (namely the solar flux and the *Kp* index) are shown in Figure 2. A closer look at these indices for each of the proposed scenarios is shown in Figure 3. On the one hand, the *Kp* index shows the variability of the ionosphere due to space weather events. On the other hand, the global electron content

Table 1. Scenario Description Table[a]

Reference	Name	Year	DOYs	# Occultations Proc.
1	High solar flux (equinox)	2011	261–267	1474
2	High solar flux (solstice)	2011	352–358	755
3	Low solar flux	2008	234–240	1185
4	Geomagnetic storm	2006	346–352	952

[a]The periods considered to generate each ionospheric scenario are listed under the *Year* and days of year, *Baseline DOYs*. The last column includes the number of FORMOSAT-3/COSMIC occultations that constitute the profile database for each scenario.

is closely correlated with the solar flux, also included, and closely follows the solar and seasonal cycles of the ionosphere, among other periodicities.

Regarding the selection of scenarios, the seasonal variation (equinox/solstice) has been considered only in the high solar activity case because the differences during low solar activity are small enough, which permits the consideration of only one season.

4.1. Scenario Occurrence Probability

As a measure of the representativeness and relevance of the proposed scenarios, the following statistical analysis has been provided in order to quantify the probability of occurrence. This analysis is based on the cumulative distribution functions (CDF) of the solar flux and *Kp* indices provided in Figure 4, computed from NOAA values during more than one solar cycle (1995 to 2015), and considering that the main parameter for classification is the solar flux for scenarios 1 to 3 and *Kp* index for Scenario 4. A discussion for each scenario is as follows:

1. Scenario 1 has been selected to contain the day with maximum solar flux value in the period with available FORMOSAT-3/COSMIC data (Figure 2), resulting in a value of 191 W/m^2/Hz (see Figure 3, top left). The value of the CDF at this point (i.e., percentile) is 92.3% (i.e., this percentage of the considered period 1995–2015 was characterized by a lower solar flux value). This indicates that this scenario is indeed representative of a very high ionization period.
2. Similarly for Scenario 2, the maximum solar flux value for this period is 141 W/m^2/Hz, which yields a percentile of 76.5%. This is also a reasonable indicator that the Scenario 2 is representative of a period with a high ionization level.
3. For Scenario 3, the opposite reasoning is applied. The minimum solar flux for this scenario period has been searched for (68 W/m^2/Hz). In this case, the percentile of days that are above this value is 72.3%. As in the case of Scenario 2, this high percentile indicates that the scenario is a good representation of a scenario with low solar activity conditions, since more than two thirds of the time from 1995 to 2015 is characterized by a higher solar flux value.

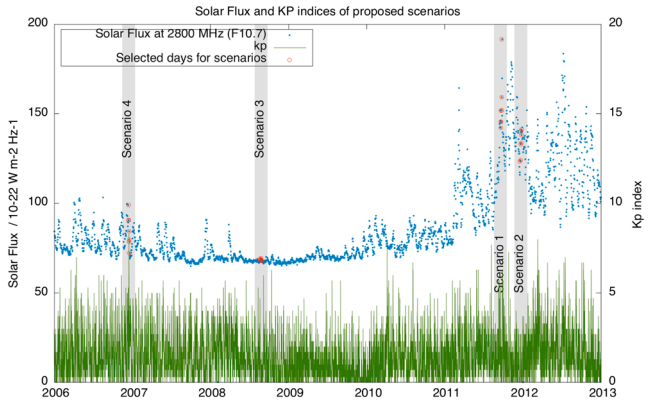

Figure 2. Solar flux ($F_{10.7}$) and *Kp* indices for each of the scenarios proposed in this study. The red circles indicate the days within each scenario, that corresponds to the days listed in Table 1.

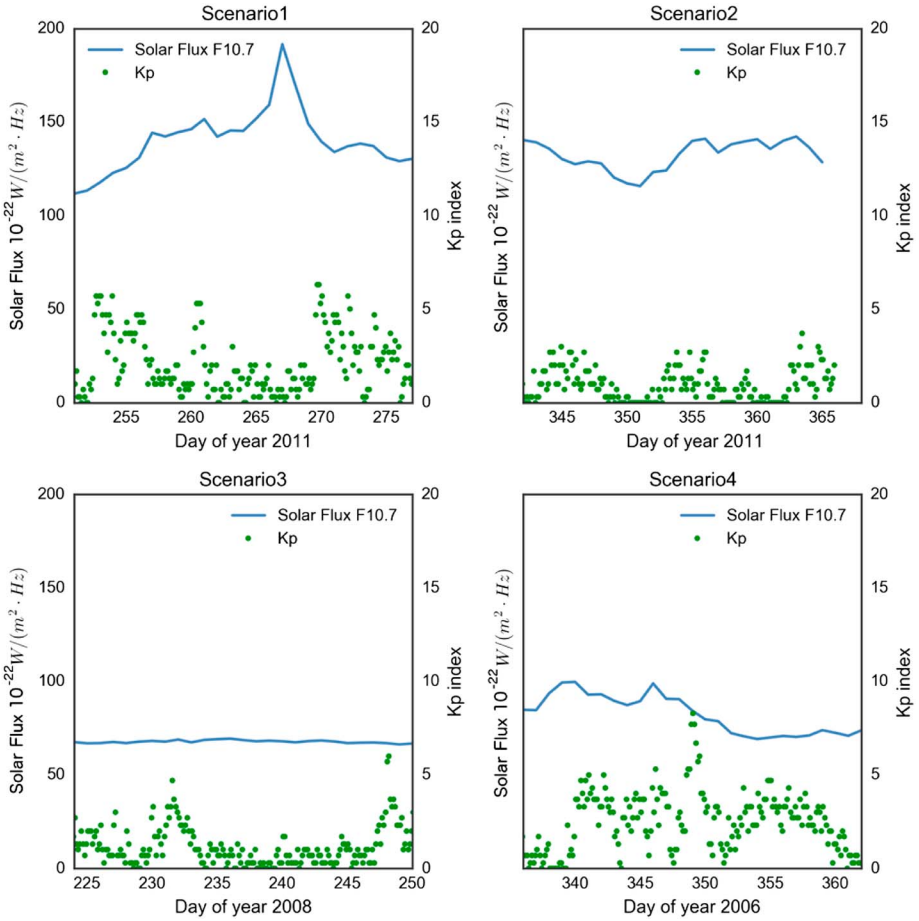

Figure 3. Solar flux ($F_{10.7}$) and *Kp* indices for each of the scenarios proposed in this study (zoom). See also Figure 2.

4. For Scenario 4, the *Kp* index is used instead of the solar flux. In this case, the maximum *Kp* value found in this period is 8.3, which yields a percentile of 99.99% (of periods with lower *Kp* index). This is indeed a clear indication that the scenario represents a rare and extreme situation in terms of ionospheric conditions.

5. Modeling and Correcting of Topside Electron Content

In order to refine the ionospheric radio-occultation inversion, a topside electron content model above FORMOSAT-3/COSMIC LEOs (>800 km) has been built, fitting a dual-layer tomographic voxel model (like in *Hernández-Pajares et al.* [1999] for ground-based GNSS observations) with the precise orbit determination

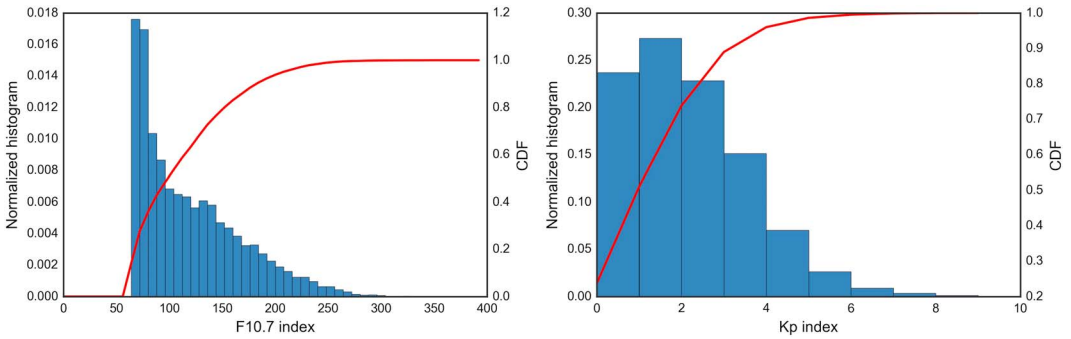

Figure 4. Histograms and cumulative distribution function (CDF) of the key parameters used to classify the scenarios: solar flux (left column) $F_{10.7}$ and (right column) *Kp* index, both from 1995 to 2015 (source: NOAA).

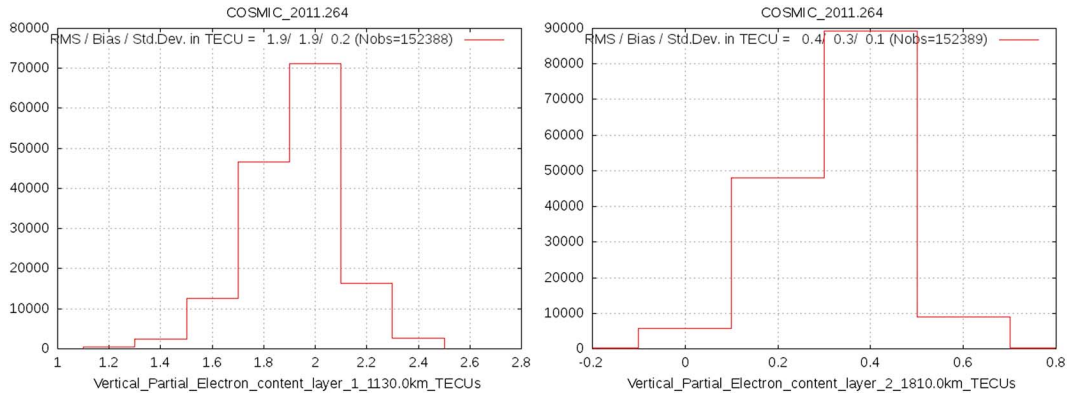

Figure 5. Distribution of FORMOSAT-3/COSMIC topside electron content estimates, (left and right) first and second shells of voxels, respectively, during day 264, 2011.

(POD) GNSS antenna measurements. This provides information on the topside as well as from the plasmasphere directly derived from the measurements, avoiding the error associated with a standard single fixed height layer mapping function. This completely new ionospheric topside electron content has been implemented and solved in a forward+backward Kalman filter, fed with all the GNSS observations taken with positive elevation angle above the local LEO horizon.

As an example, the results obtained during day 264 of year 2011 are summarized in Figure 5 where the distribution of electron content estimates in first and second layer are shown (shells centred at 1130 km and 1810 km, respectively, with a horizontal voxel dimension of 12° × 10° in right ascension and declination/latitude).

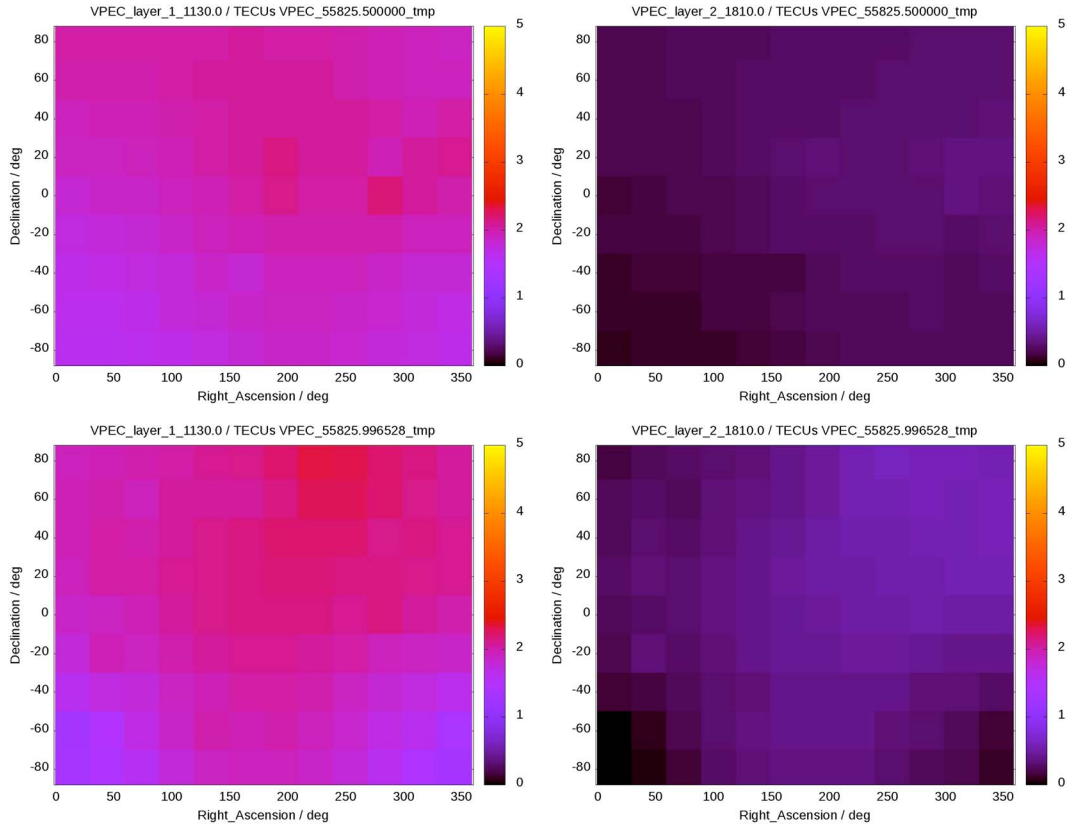

Figure 6. Topside electron content estimates (in TECUs) derived from FORMOSAT-3/COSMIC POD antenna measurements, (left and right columns) first and second shells of voxels, respectively, during day 264, 2011 at (top row) 12:00 and (bottom row) 23:55 GPS time.

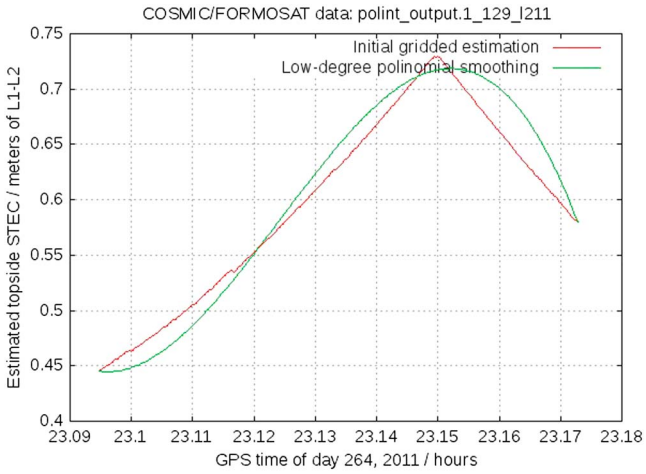

Figure 7. Example of topside slant electron content correction, during day 264.

Two snapshots of the corresponding final estimations can be found in Figure 6, where there is a smooth distribution of which the highest values (of few total electron content units (TECUs, 1 TECU = 10^{16} el m^{-2}) and tenths of TECUs for first and second layer, respectively) are distributed around the Sun position (right ascension of about 178° and latitude of 1° approximately). Moreover, the associated plasmaspheric scale heights are distributed with values in between 565 km and 1118 km, in agreement with the values derived from topside ionospheric sounders [see *Marinov et al.*, 2015] (Figure 3 (top row) in this paper).

As a direct and mainly intended application, the component of the Slant Total Electron Content (STEC) of the radio-occultation measurements, due to the ray path above the LEO orbit, is derived from such dual-layer tomographic estimations of the plasmasphere, by smoothing the topside with a low-degree polynomial. In this way, we remove the discontinuities of the derivative, associated to the grid tomographic estimation, from the ionospheric delay correction above the LEO (see Figure 7).

Finally, an example of the impact of the application of such LEO topside slant electron content corrections can be seen in Figure 8. Indeed, this shows an improvement on bottom-side electron density profile (removing negativity) after applying the dual-layer tomographic plasmaspheric correction (autonomously computed from POD FORMOSAT-3/COSMIC measurements).

6. Computations and Results

We have considered the dual-frequency FORMOSAT-3/COSMIC RO GPS measurements gathered in the four scenarios selected in the previous section. The VCET assessment has been performed as follows:

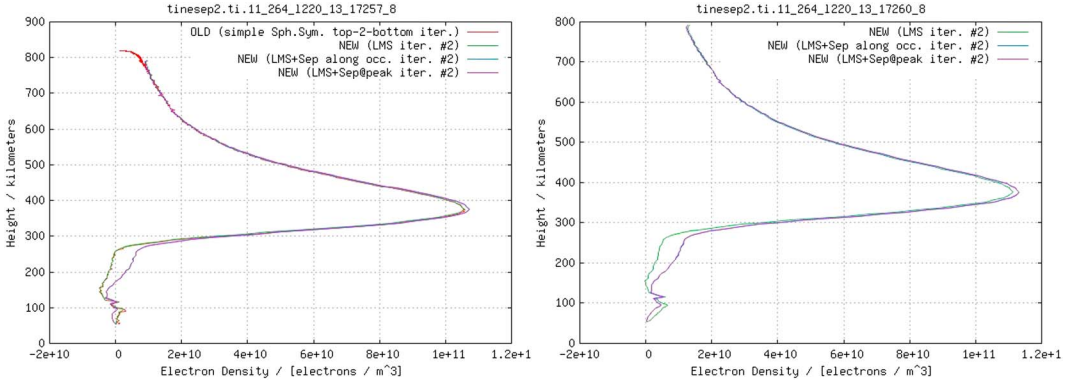

Figure 8. Electron density profile, inverted from the FORMOSAT-3/COSMIC radio-occultation measurements before (left) and after (right) applying the POD antenna measurements based plasmaspheric electron content estimation (day 264, 2011).

1. Following the approach detailed in previous section, the topside electron content model is estimated from the dual-frequency POD antenna carrier phase measurements and discounted accordingly in terms of slant ionospheric delay to all the radio-occultation measurements.
2. The EDPs are obtained for each given RO event, from the estimated shape function s characterizing each event, which typically last for few minutes and the time dependence can be ignored:

$$s(h) = \frac{N_e(h, L, \phi)}{V(L, \phi)} \tag{3}$$

where N_e is the electron density and V is the vertical total electron content (VTEC), depending on altitude h, local time L and latitude ϕ, and $s(h)$ the shape function profile (SFP). In order to better retrieve the SFP, the IATI technique has been specifically updated with respect to previous above mentioned works:

   i. V is taken from VTEC global ionospheric maps (GIMs), estimated and provided by Universitat Politècnica de Catalunya (UPC) in the context of the International GNSS Service since 1998 [*Hernández-Pajares et al.*, 1999], by using a combined tomographic and kriging technique [*Hernández-Pajares et al.*, 1999; *Orus-Perez et al.*, 2005], and probably one of the best or the best behaving GIM [see, e.g., *Feltens et al.*, 2011; *Hernández-Pajares et al.*, 2016; *Orus-Perez*, 2016].
   ii. The selection criteria to filter out unrealistic occultations are an important point as stated in *Uma et al.* [2016]. For each of the profiles, obtained after cycle-slip detection, computation of both GPS and LEO satellite positions and Abel transform inversion, a radio-occultation ionospheric profile quality control (hereinafter ROIQC) has been performed. ROIQC is based on the previous experience of the authors with GPS/MET, SAC-C, CHAMP, and FORMOSAT-3/COSMIC radio-occultation missions and consists of a first step with the following main points:
   a. A minimum height range (550 km for example) should be guaranteed in order to cover the main ionospheric layers.
   b. The integrated profile (i.e., VTEC in case of electron density) should be close to the integrated value of the absolute value (75%, for example), in order to avoid unrealistic negative values of the shape function (or electron density).
   c. The maximum relative variation of the first order profile derivative, between consecutive samples should be smaller than a certain large threshold (for instance, 2000%).
   d. The height corresponding to the maximum relative variation of the first order profile derivative (see previous point) should be smaller than a certain value (a geocentric distance of 6550 km, for instance), avoiding nonrealistic features (i.e., non–sporadic-E layer events), with curvature that is too high.
   e. The impact parameter of the profile maximum peak should be below a certain maximum reasonable value, in concordance with the LEO orbital height and expected electron content vertical distribution (e.g., 7000 km).

   In addition, a second filtering step of the resulting profiles is applied to further minimize the unrealistic variability events:
   a. A strict positivity is required for all the points of the profile.
   b. The profiles containing any outlier regarding the distribution of the first- and second-order vertical derivative of the shape function/electron density, for each one of the eight sectors of the profile (defined by boundaries at heights of 0, 70, 150, 250, 350, 450, 550, 650, 1000 km), are rejected.
3. The VCET is applied per occultation event as described in the corresponding sections above. The top height of data availability has been taken as $h_1 = 500$ km, corresponding to the mission constraints. The minimum height value h_0 for linearly fitting the local-scale height values H is considered as $h_mF_2 + 100$ km, in order to avoid linear model worsening very close to the electron density profile peak (see again *Olivares-Pulido et al.*, 2016 for details) but still allocating the majority of occultation events (see Figure 1 with less than 0.1% of the overall profiles presenting a peak height above 500 km—corresponding to two cases with exceptionally low electron density values).
4. Finally, three additional approaches, variants of the *classical* Chapman model, have been considered for comparison, by estimating the constant topside scale height in three different ways:
   i. The first approach is a *climatic* estimate provided by the Capellari model [*Cappellari et al.*, 1976], applicable (similarly to VCET) for the actual extrapolation problem [see also *Feltens*, 1998]. It is assumed that the scale height H shows a constant linear dependence with the F2 layer peak height h_mF_2:

$$H = \frac{1}{3}(h_mF_2 - 50\,\text{km}) \tag{4}$$

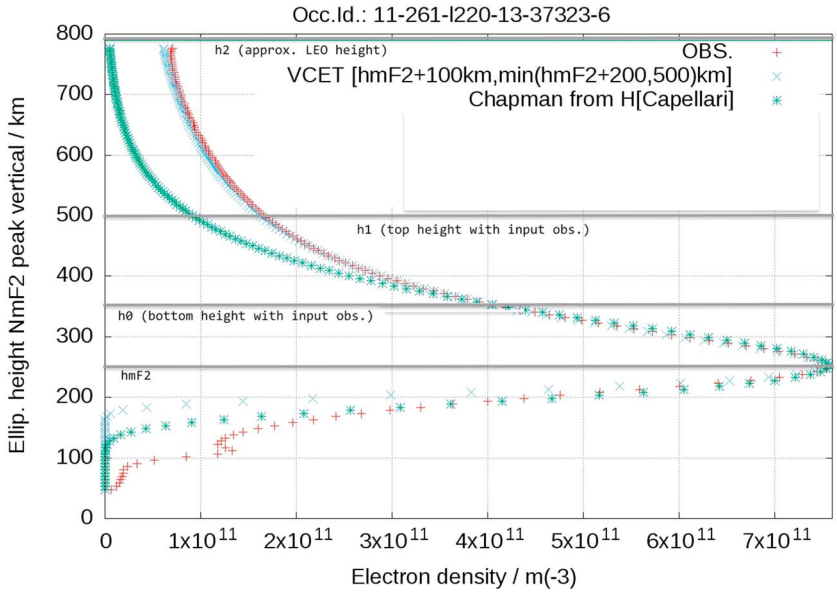

Figure 9. This shows one typical example of VCET performance (blue squares) vs the one of Capellari-based Chapman extrapolation (green stars), both compared with the measured electron density values estimated by updated IATI (red crosses), within the extrapolation range $[h_1, h_2]$ (the remaining relevant heights in the extrapolation problem, such as the bottom height to fit the linear Vary-Chap model, h_0, and the F2 layer peak height h_mF_2, are also indicated). The input data (raw dual-frequency carrier phase measurements) correspond to GPS PRN13 occultation measured from the FORMOSAT-3/COSMIC LEO #2, antenna 0, approximately at 10:22 GPS time of the day 261 of year 2011.

ii. The second approach is a classical α-Chapman model, in which the topside constant height is derived from the available N_mF_2 values, and the ionospheric VTEC (V_I, by integrating the overall EDP up to the LEO height $0 \le h \le h_2$, following equation (1), making the change $y = e^{-z/2}/\sqrt{2}$ and extending the limit to infinity), by means of the relationship:

$$V_I = \int_{h=0}^{h_2} N \cdot dh \simeq e^{\frac{1}{2}} \sqrt{2\pi} N_m F_2 \cdot H \Longrightarrow H \simeq \frac{V_I}{e^{\frac{1}{2}} \sqrt{2\pi} N_m F_2} \tag{5}$$

In principle, this approach might not be used in the realistic extrapolation scenario (V_I), because it uses information for $h > h_1$ not available (the V_I by integrating the full EDP up to the LEO altitude).

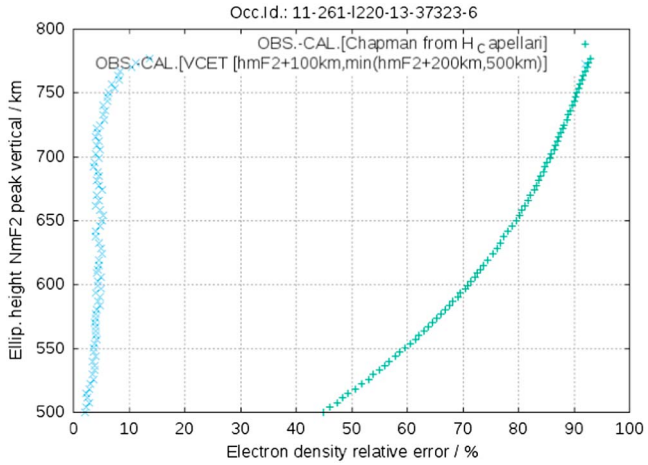

Figure 10. Relative error (percentage) of VCET (blue points) vs the one of Capellari based on Chapman extrapolation (green points), both compared with the measured electron density values estimated by updated IATI (occultation corresponding to the EDP shown in previous Figure 9).

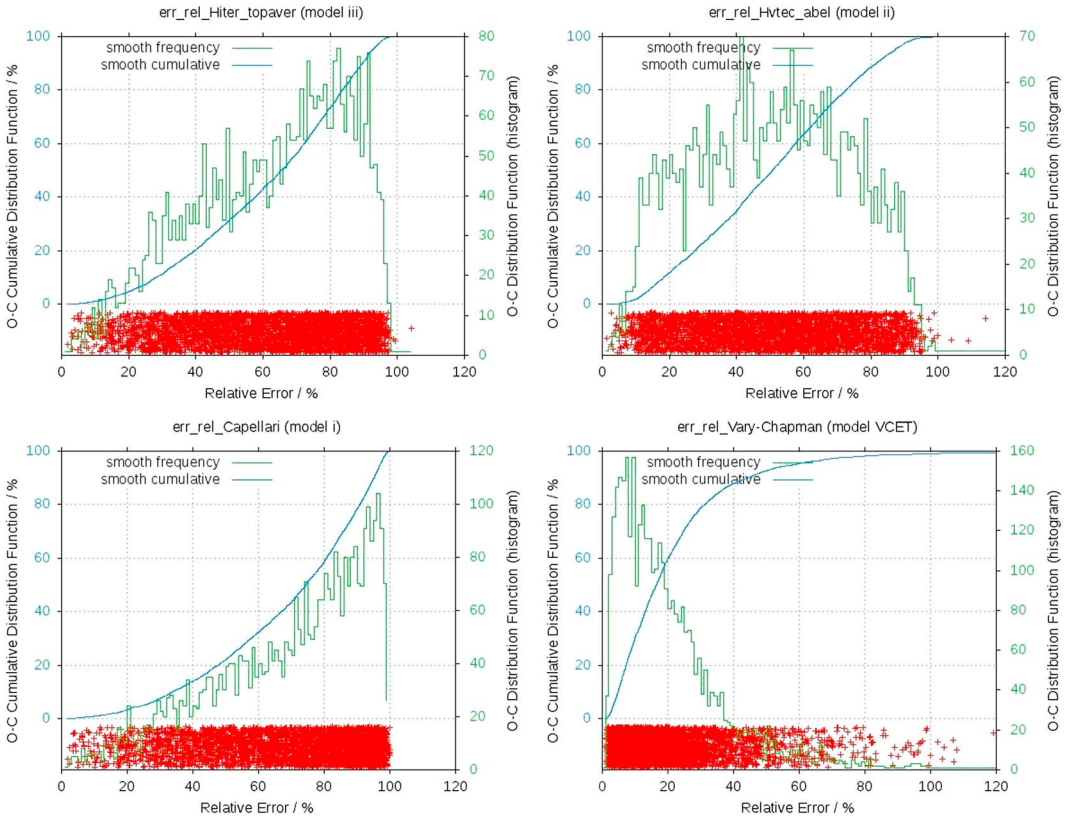

Figure 11. Distribution of relative error (frequency and cumulative distributions, in green and blue lines, respectively, and random realization in red crosses) of Chapman models with topside-scale height obtained from (bottom left) (i) the observed averaged values, (top right) (ii) from VTEC, N_mF_2, and Chapman relationship, (top left) (iii) from Capellari relationship (actual extrapolation), and (bottom right) applying VCET. The results have been obtained on +3700 occultations estimated with updated IATI in four selected scenarios.

Nevertheless, such information might be indirectly derived from the overall VTEC (provided by the GIM from ground-based GPS receivers up to the GPS transmitters altitude, V) and the VTEC observed above the LEO height from the POD antenna measurements, V_P ($V_I = V - V_P$).

iii. The third approach is a model which should in principle be better than VCET, because it is not extrapolating at all, is the classical Chapman model based on the average of the reference topside scale height local values for $h_1 \leq h \leq h_2$, derived from the full EDP directly observed such as the case of FORMOSAT-3/COSMIC GPS receivers. Nevertheless, this approach might not be available in future missions focusing on neutral atmospheric sounding.

Figure 9 shows one typical example of performance for the VCET and Chapman-Capellari extrapolation technique, firstly listed above (blue and green data, respectively), compared with the reference EDP obtained with the full FORMOSAT-3/CHAPMAN measurements. Their relative errors with respect to the observational data are displayed in Figure 10. It can be seen that the VCET method performs better than the Chapman-Capellari technique.

The overall results for the four above mentioned techniques can be found in Figure 11, in which it is seen that VCET is more accurate than the other extrapolation techniques (Chapman model based on the Capellari climatic scale height) and also performs better than the other approaches using topside measurements, with relative error probability peak of VCET at 7%–10%, whereas it is about 40%, 80%, and 95% for classical Abel implementations (ii), (iii), and (i) (with scale heights given from the average of topside values, from the VTEC, and by Capellari relationship, respectively). Namely, 60% of EDPs present an extrapolation relative error smaller than 20% with VCET, whereas the best performed classical Chapman model (based on the constant topside scale height dependence on VTEC and F2 electron density peak) provides 10% of profiles presenting a relative error below 20%. All these comparisons are very significant, taking into account that the relative IATI technique used to provide the reference profiles presents relative error better than 9–28% at h_mF_2

(see assessments with ionosonde data in *Hernández-Pajares et al.* [2000] and *Garcia-Fernàndez et al.* [2003]), and that the IATI accuracy at the target heights in this work should be still more accurate (above 500 km, i.e., closer to the LEO GNSS receiver than h_mF_2).

These results are well maintained when the maximum available SLTA value, h_2, is increased: just a slight overall improvement (reduction of relative error of about 2%) is obtained for $h_2 = 550$ km, compared with the EPS-SG case of $h_2 = 500$ km studied in this work. This last result is compatible with the accurate description given by the Vary-Chapman model under the assumption of scale height linearly dependent with the altitude at the topside part of the EDP, as detailed in *Olivares-Pulido et al.* [2016].

7. Conclusions

A new Vary-Chap-based Extrapolation Technique of electron density (VCET), physically consistent with the linear temperature increase above h_mF_2, has been developed. VCET is based on the Vary-Chap linear model of the topside scale height, and it is suitable for processing and extrapolating the electron density profiles above 500 km of height, presenting a performance much better than other approaches based on the classical Chapman model.

The VCET performance has been assessed with actual FORMOSAT-3/COSMIC measurements during four representative weeks of different ionospheric conditions: solar flux maximum and minimum, and major and quiet geomagnetic activity. It is found that with VCET, 60% of the occultations can be extrapolated with less than 20% relative error above 500 km and up to the LEO height (800 km approximately). However, only 3–10% of the occultations can be extrapolated with such relative error smaller than 20% when different implementations of the classical Chapman model (assuming constant scale height) are considered. It is worth mentioning that the reference profiles of the overall comparisons have been generated accurately with an updated version of the Improved Abel Transform Inversion applied to the radio-occultation measurements. It includes in particular a previous direct tomographic determination, and corresponding radio-occulation correction, of the LEO topside electron content, performed from the GNSS POD antenna measurements.

Acknowledgments
The data for this work are available, and they can be requested from the authors, in particular from Manuel Hernández-Pajares (manuel.Hernandez@upc.edu). This work has been partially performed in the context of the ROPE project funded by EUMETSAT (contract EUM/CO/15/4600001591/AVE). The authors are grateful to Taiwan Science and UCAR, which are responsible for FORMOSAT-3/COSMIC measurements.

References

Alizadeh, M. M., H. Schuh, and M. Schmidt (2015), Ray tracing technique for global 3-D modeling of ionospheric electron density using GNSS measurements, *Radio Sci.*, *50*, 539–553, doi:10.1002/2014RS005466.

Anthes, R. A., et al. (2008), The COSMIC/FORMOSAT-3 mission: Early results, *Bull. Am. Meteorol. Soc.*, *89*(3), 313–333.

Aragón-Àngel, A., Y. A. Liou, C. C. Lee, B. W. Reinisch, M. Hernández-Pajares, M. Juan, and J. Sanz (2011), Improvement of retrieved FORMOSAT-3/COSMIC electron densities validated by ionospheric sounder measurements at Jicamarca, *Radio Sci.*, *46*, RS5001, doi:10.1029/2010RS004578.

Cappellari, J. O., C. E. Velez, and A. J. Fuchs (1976), Mathematical theory of the goddard trajectory determination system, Tech. Rep. NASA-TM-X-71106, X-582-76-77, Goddard Space Flight Cent., Greenbelt, Md., April 1976, Section 7.6.2, "Ionosphere Models", pp. 7-44–7-52.

Danzer, J., S. B. Healy, and I. D. Culverwell (2015), A simulation study with a new residual ionospheric error model for GPS radio occultation climatologies, *Atmos. Meas. Tech.*, *8*(8), 3395–3404.

Feltens, J. (1998), Chapman profile approach for 3-D global TEC representation, paper presented at IGS Analysis Workshop, ESOC, Darmstadt, Germany, Feb. 1998.

Feltens, J., M. Angling, N. Jackson-Booth, N. Jakowski, M. Hoque, M. HernándezPajares, A. Aragón-Àngel, R. Orus-Perez, and R. Zandbergen (2011), Comparative testing of four ionospheric models driven with GPS measurements, *Radio Sci.*, *46*, RS0D12, doi:10.1029/2010RS004584.

Garcia-Fernàndez, M., M. Hernández-Pajares, M. Juan, and J. Sanz (2003), Improvement of ionospheric electron density estimation with GPSMET occultations using Abel inversion and VTEC information, *J. Geophys. Res.*, *108*(A9), 1338, doi:10.1029/2003JA009952.

Garcia-Fernàndez, M., M. Hernandez-Pajares, J. M. Juan, and J. Sanz (2005a), Performance of the improved Abel transform to estimate electron density profiles from GPS occultation data, *GPS Solutions*, *9*(2), 105–110.

Garcia-Fernàndez, M., A. Saito, J. M. Juan, and T. Tsuda (2005b), Three-dimensional estimation of electron density over Japan using the GEONET GPS network combined with SAC-C data and ionosonde measurements, *J. Geophys. Res.*, *110*, A11304, doi:10.1029/2005JA011037.

González-Casado, G., J. M. Juan, J. Sanz, A. Rovira-Garcia, and A. Aragón-Àngel (2015), Ionospheric and plasmaspheric electron contents inferred from radio occultations and global ionospheric maps, *J. Geophys. Res. Space Physics*, *120*, 5983–5997, doi:10.1002/2014JA020807.

Hajj, G. A., and L. J. Romans (1998), Ionospheric electron density profiles obtained with the Global Positioning System: Results from the GPS/MET experiment, *Radio Sci.*, *33*(1), 175–190.

Hernández-Pajares, M., J. M. Juan, J. Sanz, and J. G. Sole (1998), Global observation of the ionospheric electronic response to solar events using ground and LEO GPS data, *J. Geophys. Res.*, *103*(A9), 20,789–20,796.

Hernández-Pajares, M., J. M. Juan, and J. Sanz (1999), New approaches in global ionospheric determination using ground GPS data, *J. Atmos. Sol. Terr. Phys.*, *61*(16), 1237–1247.

Hernández-Pajares, M., J. M. Juan, and J. Sanz (2000), Improving the Abel inversion by adding ground GPS data to LEO radio occultations in ionospheric sounding, *Geophys. Res. Lett.*, *27*(16), 2473–2476.

Hernández-Pajares, M., et al. (2016), Comparing performances of seven different global VTEC ionospheric models in the IGS context, IGS WS, Sydney, Australia, 8–12 Feb. [Available at http://www.igs.org/assets/pdf/W2016%20-%20PY0507%20-%20Hernandez-Pajares.pdf.]

Jakowski, N., A. Wehrenpfennig, S. Heise, C. Reigber, H. Lühr, L. Grunwaldt, and T. K. Meehan (2002), GPS radio occultation measurements of the ionosphere from CHAMP: Early results, *Geophys. Res. Lett.*, *29*(10), 1457, doi:10.1029/2001GL014364.

Kutiev, I., P. Marinov, and A. Belehaki (2016), Real time 3-D electron density reconstruction over Europe by using TaD profiler, *Radio Sci.*, *51*, 1176–1187, doi:10.1002/2015RS005932.

Lee, H.-B., Y. H. Kim, E. Kim, J. Hong, and Y.-S. Kwak (2016), Where does the plasmasphere begin? Revisit to topside ionospheric profiles in comparison with plasmaspheric TEC from Jason-1, *J. Geophys. Res. Space Physics*, *121*, 10,091–10,102, doi:10.1002/2016JA022747.

Liu, L., M. He, W. Wan, and M.-L. Zhang (2008), Topside ionospheric scale heights retrieved from Constellation Observing System for Meteorology, Ionosphere, and Climate radio occultation measurements, *J. Geophys. Res.*, *113*, A10304, doi:10.1029/2008JA013490.

Luntama, J. P. (2005), Ionosphere monitoring with Metop GRAS mission, paper presented at 2nd European Space Weather Week, European Space Agency, Noordwijk, Netherlands.

Mannucci, A. J., C. O. Ao, X. Pi, and B. A. Iijima (2011), The impact of large scale ionospheric structure on radio occultation retrievals, *Atmos. Meas. Tech.*, *4*(12), 2837–2850.

Marinov, P., I. Kutiev, A. Belehaki, and I. Tsagouri (2015), Modeling the plasmasphere to topside ionosphere scale height ratio, *J. Space Weather Space Clim.*, *5*, A27.

Nsumei, P., B. W. Reinisch, X. Huang, and D. Bilitza (2012), New Vary-Chap profile of the topside ionosphere electron density distribution for use with the IRI model and the GIRO real time data, *Radio Sci.*, *47*, RS0L16, doi:10.1029/2012RS004989.

Olivares-Pulido, G., M. Hernández- Pajares, A. Aragón-Àngel, and A. Garcia-Rigo (2016), A linear scale height Chapman model supported by GNSS occultation measurements, *J. Geophys. Res. Space Physics*, *121*, 7932–7940, doi:10.1002/2016JA022337.

Orus-Perez, R. (2016), Ionospheric error contribution to GNSS single-frequency navigation at the 2014 solar maximum, *J. Geod.*, *91*(4), 397–407.

Orus-Perez, R., M. Hernández-Pajares, J. M. Juan, and J. Sanz (2005), Improvement of global ionospheric VTEC maps by using kriging interpolation technique, *J. Atmos. Sol. Terr. Phys.*, *67*(16), 1598–1609.

Rius, A., G. Ruffini, and A. Romeo (1998), Analysis of ionospheric electron density distribution from GPS/MET occultations, *IEEE Trans. Geosci. Remote Sens.*, *36*(2), 383–394.

Ruffini, G., E. Cardellach, A. Flores, L. Cucurull, and A. Rius (1998), Ionospheric calibration of radar altimeters using GPS tomography, *Geophys. Res. Lett.*, *25*(20), 3771–3774.

Schreiner, W. S., S. V. Sokolovskiy, C. Rocken, and D. C. Hunt (1999), Analysis and validation of GPS/MET radio occultation data in the ionosphere, *Radio Sci.*, *34*(4), 949–966.

Su, F., W. Wang, A. G. Burns, X. Yue, and F. Zhu (2015), The correlation between electron temperature and density in the topside ionosphere during 2006–2009, *J. Geophys. Res. Space Physics*, *120*, 10,724–10,739, doi:10.1002/2015JA021303.

Tulasi Ram, S., S.-Y. Su, C. H. Liu, B. W. Reinisch, and L.-A. McKinnell (2009), Topside ionospheric effective scale heights (H_T) derived with ROCSAT-1 and ground-based ionosonde observations at equatorial and midlatitude stations, *J. Geophys. Res.*, *114*, A10309, doi:10.1029/2009JA014485.

Uma, G., P. S. Brahmanandam, and Y. H. Chu (2016), A long-term study on the deletion criterion of questionable electron density profiles caused by ionospheric irregularities—COSMIC radio occultation technique, *Adv. Space Res.*, *57*(12), 2452–2463.

Zeng, Z., S. Sokolovskiy, W. Schreiner, D. Hunt, J. Lin, and Y.-H. Kuo (2016), Ionospheric correction of GPS radio occultation data in the troposphere, *Atmos. Meas. Tech.*, *9*, 335–346, doi:10.5194/amt-9-335-2016. [Available at http://www.atmos-meas-tech.net/9/335/2016/.]

Zhu, Q., J. Lei, X. Luan, and X. Dou (2016), Contribution of the topside and bottomside ionosphere to the total electron content during two strong geomagnetic storms, *J. Geophys. Res. Space Physics*, *121*, 2475–2488, doi:10.1002/2015JA022111.